Polyhedron xxx (2014) xxx–xxx

Contents lists available at ScienceDirect

Polyhedron

journal homepage: www.elsevier.com/locate/poly

Synthesis, structure and magnetic properties of a series of cubane-like clusters derived from Schiff base ligands

Xiaoting Qin, Shuai Ding, Xuebin Xu, Rui Wang, Ye Song, Yanqin Wang, Chun-fang Du, Zhi-liang Liu *

Key Lab of Nanoscience and Nanotechnology, College of Chemistry and Chemical Engineering, Inner Mongolia University, Hohhot 010021, PR China

ARTICLE INFO

Article history:
Received 25 January 2014
Accepted 22 March 2014
Available online xxxx

Keywords:
Compounds
Cubane
Schiff base
Magnetic properties
Crystal structures

ABSTRACT

One new hexanuclear Cu(II) complex $[Cu_4(L^1)_4Na_2(ClO_4)(H_2O)](ClO_4)(H_2O)_{0.5}$ (**1**) and two new tetranuclear Ni(II) complexes $[Ni_4(L^2)_4(CH_3OH)_4]$ (**2**), $[Ni_4(o\text{-vanillinate})_4(\mu_3\text{-}N_3)_4(CH_3OH)_4]$ (**3**) have been synthesized and structurally characterized. All the three complexes **1**, **2**, and **3** have been characterized by elemental analysis, FTIR, and single crystal X-ray diffraction studies. Single crystal X-ray diffraction studies reveal that all three complexes consist of a cubane core in which the four Cu(II)/Ni(II) centers in **1** and **2** are linked by μ_3-alkoxo bridges and Ni(II) ions in **3** are linked by azido bridge in end-on fashion. The skeleton structures of the cubane cores are all distorted from the idealized cube and most show a further distortion. The variable-temperature (2–300 K) magnetic susceptibilities and magnetizations of the three compounds were measured. Variable-temperature magnetic susceptibility data exhibit dominant antiferromagnetic interaction in complex **1** while ferromagnetic interactions in complexes **2** and **3**.

1. Introduction

To design coordination complexes of copper(II) and nickel(II) is now ubiquitous in the field of condensed matter physics and material chemistry [1–4]. In the family of above mentioned complexes, cubane-like clusters are amazing metalloclusters that have received great attention during the past decade, for the potential bioinorganic modeling, catalysis and hydrogenases [5,6]. Several cubane-like Cu(II)/Ni(II) complexes containing μ_3-O bridges have been extensively studied, mainly stimulated by their significant contribution to the field of molecular magnetism [7–19]. In terms of Ni(II) cubane complexes bridged by end-on bridging azides which possess similar $[Ni_4(\eta^1,\mu_3\text{-}N_3)_4]$ cubane cores, only three examples have been reported [20–23].

Recently, a series of Schiff base ligands as building blocks have been used to synthesize the cubane-like 3d transition metal clusters and most of them provide alkoxo-bridges between metallic centers. The ligands containing three and four potential donor groups, such as 2-((1-hydroxybutan-2-ylimino)methyl)-6-methoxyphenol (H_2L^1), 2-((1-hydroxybutan-2-ylimino)methyl)phenol (H_2L^2) and 2-((2-hydroxyethylimino)methyl)-6-methoxyphenol (H_2L^3, see Scheme 1), consequently, were considered as excellent organic blocking ligands because of their various coordination modes, such as M_4 arrays, which exhibit a large diversity of structure types: square planar, [24] face-to-face, [25] cyclic [26] and cubane type [27–30]. M_4O_4 units show interesting magnetic exchange properties and may under certain circumstances act as single molecular magnets [31]. The diverse structures and interesting properties observed in these compounds attract us to do some further research about these interesting ligands. Indeed, ligand H_2L^1 has previously been utilized in the assembly of the mononuclear zinc complex and the binuclear nickel complex [32,33]. Ligand H_2L^2 has been explored to construct a mononuclear titanium complex [34] and a dinuclear nickel complex [35]. Ligand H_2L^3 has been reported to construct 3d transition metal clusters with various core structures, such as Co_1, Ni_2, Cu_4, Ni_4 [36–41]. A Cambridge Structural Database search reveals that so far few of cubane-like clusters, however, using these Schiff base ligands, have been known and little comparative discussed. In order to enrich the family of cubane-like clusters, we have successfully obtained three new cubane-like clusters, namely, $[Cu_4(L^1)_4Na_2(ClO_4)(H_2O)](ClO_4)(H_2O)_{0.5}$ (**1**), $[Ni_4(L^2)_4(CH_3OH)_4]$ (**2**), $[Ni_4(o\text{-vanillinate})_4(\mu_3\text{-}N_3)_4(CH_3OH)_4]$ (**3**). Variable-temperature magnetic susceptibility data exhibit antiferromagnetic interaction in complex **1** while dominant ferromagnetic interactions in complexes **2** and **3** exist in the cubane core, and magnetostructural correlations were discussed furthermore.

2. Material and methods

2.1. Materials

All reagents and solvents were of high-purity analytical grade and used as received from commercial supplies without further

* Corresponding author. Tel.: +86 471 4995414; fax: +86 471 4992147.
E-mail address: cezlliu@imu.edu.cn (Z.-l. Liu).

http://dx.doi.org/10.1016/j.poly.2014.03.040
0277-5387/

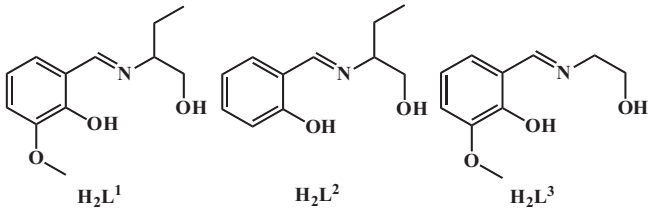

Scheme 1. The structure of the Schiff base ligands (H_2L^1, H_2L^2 and H_2L^3).

purification. Ethanolamine, 2-amin-1-butanol, salicylaldehyde, o-vanillin, $Cu(ClO_4)_2{\cdot}6H_2O$, $Ni(ClO_4)_2{\cdot}6H_2O$ and all the solvents were purchased from Aladdin and Alfa Aesar, respectively. The Schiff base ligands H_2L^1, H_2L^2 and H_2L^3 were synthesized according to literature procedures [33,37,42].

2.2. Synthesis of complex

2.2.1. $[Cu_4(L^1)_4Na_2(ClO_4)(H_2O)](ClO_4)(H_2O)_{0.5}$ (**1**)

$Cu(ClO_4)_2{\cdot}6H_2O$ (0.37 g, 1 mmol) was added to a solution of H_2L^1 (1 mmol) and NaOH (0.08 g, 2 mmol) in 15 ml methanol/dichloromethane (1:2 v/v), the resulting filtered solution was left unperturbed to allow a slow evaporation of the solvent. After 3 days, dark blue block-shaped crystals, suitable for X-ray diffraction analysis, were obtained. Yield: 0.056 g (16%). *Anal.* Calc. for $C_{48}H_{63}Cu_4N_4O_{21.5}Cl_2Na_2$: C, 40.89; H, 4.43; N, 3.97. Found: C, 40.66; H, 4.34; N, 3.85%. IR (KBr, cm^{-1}): 3418 (w), 2918 (m), 2850 (w), 1634 (s), 1550 (m), 1443 (s), 1306 (w), 1242 (w), 1170 (s), 1104 (w), 1014 (w), 975 (w), 848 (m), 785 (s), 622 (w).

2.2.2. $[Ni_4(L^2)_4(CH_3OH)_4]$ (**2**)

$Ni(ClO_4)_2{\cdot}6H_2O$ (0.366 g, 1 mmol) was added to a solution of H_2L^2 (1 mmol) and Et_3N (0.202 g, 2 mmol) in 15 ml methanol/dichloromethane (1:2 v/v), the resulting filtered solution was left unperturbed to allow a slow evaporation of the solvent. After 3 days, green block-shaped crystals, suitable for X-ray diffraction analysis, were obtained. Yield: 0.08 g (28%). *Anal.* Calc. for $C_{48}H_{68}Ni_4N_4O_{12}$: C, 51.11; H, 6.07; N, 4.98. Found: C, 51.50; H, 6.38; N, 4.37%. IR (KBr, cm^{-1}): 3641 (w), 2931 (m), 2859 (w), 1632 (s), 1599 (m), 1447 (s), 1391 (w), 1336 (m), 1187 (m), 1061 (m), 942 (w), 907 (m), 758 (s), 651 (w), 521 (m).

2.2.3. $[Ni_4(o\text{-vanillinate})_4(\mu_3\text{-}N_3)_4(CH_3OH)_4]$ (**3**)

$Ni(ClO_4)_2{\cdot}6H_2O$ (0.366 g, 1 mmol) was readily dissolved in 15 ml methanol, resulting in a green solution. Schiff base ligand H_2L^3 (1 mmol) and NaN_3 (0.13 g, 2 mmol) were dissolved in 15 ml methanol, resulting in a yellow solution. In a 50 ml H-shaped tube, the filtered green solution and filtered yellow solution were added dropwise to each branch of the tube, respectively. Additional 10 ml methanol was distributed and layered upon the mixture to allow a slow diffuse of the solutes. After 2 months, light green block-shaped crystals, suitable for X-ray diffraction analysis, were obtained. Yield: 0.11 g (35%). *Anal.* Calc. for $C_{36}H_{44}N_{12}Ni_4O_{16}$: C, 38.08; H, 3.91; N, 14.80. Found: C, 38.12; H, 3.93; N, 14.83%. IR (KBr, cm^{-1}): 3632 (w), 2924 (w), 2861(w), 2087 (s), 1670(s), 1577(s), 1447 (s), 1338 (m), 1236 (w), 1089 (w), 942 (m), 847 (w), 748 (m).

2.3. Physical measurements

Fourier transform infrared (FTIR) spectra (KBr disk) were measured with a Vertex 70 FTIR on a spectrophotometer (4000–400 cm^{-1}). Elemental analyses for C, H and N were obtained from a Perkin-Elmer 2400 elemental analyzer. Magnetic susceptibility was measured in the temperature range of 2–300 K using a Quantum Design MPMS XL-5 SQUID magnetometer equipped with 5 T. According to Pascal's constants, the diamagnetic corrections were made and magnetic data were corrected for diamagnetic contributions of the sample holder.

2.4. X-ray crystallography

Single crystals of the complexes were selected and mounted on a Bruker ApexII CCD diffractometer with graphite-monochromated Mo Kα radiation (λ = 0.71073 Å), operating in ω–2θ scanning mode using suitable crystals for data collection. Lorentz-polarization correction was applied to the data. The structure was solved by direct methods (SHELX-97) and refined by full-matrix least-squares procedures on F^2 using SHELX-97 [43]. Hydrogen atoms were added theoretically and refined with riding model position parameters and fixed isotropic thermal parameters. Experimental details for the structural determinations are summarized in Table 1.

3. Results and discussion

3.1. Syntheses and IR spectra of the complexes

The ligands were synthesized by condensation of 2-hydroxybenzaldehyde, or its derivative o-vanillin, with corresponding amino alcohol under refluxing in the methanol solution. The resulting orange yellow solution containing the required product was used without further purification. Suitable crystals of hexanuclear complex $[Cu_4(L^1)_4Na_2(ClO_4)(H_2O)](ClO_4)(H_2O)_{0.5}$ (**1**) and tetranuclear complex $[Ni_4(L^2)_4(CH_3OH)_4]$ (**2**) were synthesized from corresponding Schiff base ligands (H_2L^1, H_2L^2) and $M(ClO_4)_2{\cdot}6H_2O$ ($M = Cu^{2+}$, Ni^{2+}) in methanol/dichloromethane (1:2 v/v) under basic conditions to promote deprotonation and subsequent coordination of the phenoxyl and alkoxyl groups. For the reaction of $Ni(ClO_4)_2{\cdot}6H_2O$ and H_2L^3, slow diffusion in a H-tube tube at room temperature of a methanolic solution of $Ni(ClO_4)_2{\cdot}6H_2O$ into a methanolic solution of H_2L^3 and NaN_3 resulted in light green block-shaped crystals of general formula $[Ni_4(o\text{-vanillinate})_4(\eta^1,\mu_3\text{-}N_3)_4(CH_3OH)_4]$. However, it is noteworthy that, according to X-ray crystallographic analysis, o-vanillin coordinates to nickel ion instead of ligand H_2L^3. This may be attributed to the Schiff base ligand H_2L^3 decomposed during the assemble process.

The structures of **1**–**3** were characterized by infrared (IR) spectra, which showed valuable information about the counter ions in their respective coordination environments. The peak at 1634 cm^{-1} for **1**, 1632 cm^{-1} for **2** and 1670 cm^{-1} for **3** can be reasonably attributed to stretching vibrations of imino C=N and C=O groups, respectively. In the IR spectra of **1**, the strong peak at 1170 cm^{-1} should be ascribed to the presence of perchlorate anion. For complex **3**, the IR spectra exhibit strong abortion at 2087 cm^{-1}, which is due to the vibration of N_3^- anion.

3.2. Structure description

3.2.1. Crystal structure of $[Cu_4(L^1)_4Na_2(ClO_4)(H_2O)](ClO_4)(H_2O)_{0.5}$ (**1**)

X-ray single crystal diffraction analysis reveals that complex **1** crystallizes in the triclinic space group $P\bar{1}$. Each of the unit cells comprises of one cationic complex unit $[Cu_4(L^1)_4Na_2(ClO_4)(H_2O)]^+$, one isolated ClO_4^- counterion and half a crystallization water. Perspective views of the cationic complex unit are depicted in Fig. 1. Some selected bond lengths and angles are presented in Table 2.

The structure of the cationic complex $[Cu_4(L^1)_4Na_2(ClO_4)(H_2O)]^+$ in complex **1** can be described as hexanuclear skeleton ($Cu_4O_4Na_2O_4$), around which the four tetradentate Schiff base ligands $(L^1)^{2-}$ are oriented mutually staggered. The four deprotonated butanol

Table 1
Crystallographic data and structure refinement for complexes **1**–**3**.

	1	2	3
Empirical Formula	$C_{48}H_{63}Cl_2Cu_4N_4Na_2O_{21.5}$	$C_{48}H_{68}Ni_4N_4O_{12}$	$C_{36}H_{44}N_{12}Ni_4O_{16}$
Formula weight	1410.10	1127.90	1135.67
T (K)	293(2)	296(2)	296(2)
Crystal system	triclinic	monoclinic	tetragonal
Space group	$P\bar{1}$	P_{21}/c	I_{41}/a
a (Å)	11.716(2)	19.917(10)	22.347(19)
b (Å)	14.681(3)	15.218(8)	22.347(19)
c (Å)	17.556(3)	16.904(9)	9.536(17)
α (°)	95.61(3)	90.00	90.00
β (°)	90.91(3)	90.46(10)	90.00
γ (°)	101.42(3)	90.00	90.00
V (Å^3)	2943.8(9)	5123.4(5)	4761.9(10)
Z	2	4	4
ρ_{calc} (g cm–3)	1.591	1.462	1.584
Absorption coefficient (mm^{-1})	1.609	1.510	1.636
F (000)	1444	2368	2336.0
θ Range (°)	1.59 < θ < 25	1.02 < θ < 25.02	3.64 < θ < 56.68
Reflections collected	30470	26038	14528
Unique reflections	10296	9019	2967
R_{int}	0.0543	0.0489	0.0328
Goodness-of-fit (GOF) on F^2	1.063	1.031	1.072
Final R indices [$I > 2\sigma(I)$]	R^a = 0.0618 wR^b = 0.1654	R^a = 0.0402, wR^b = 0.0863	R^a = 0.0461 wR^b = 0.1313
R indices (all data)	R = 0.0717 wR = 0.1741	R = 0.0652 wR = 0.0980	R = 0.0781 wR = 0.1538
Largest residuals (e Å^{-3})	1.34 and −0.86	0.723 and −0.098	0.72 and −0.67

[a] $R = \Sigma||F_0| - |F_c||/\Sigma|F_0|$.
[b] $wR = [\Sigma w(F_0^2 - F_c^2)^2/\Sigma(wF_0^4)]^{1/2}$.

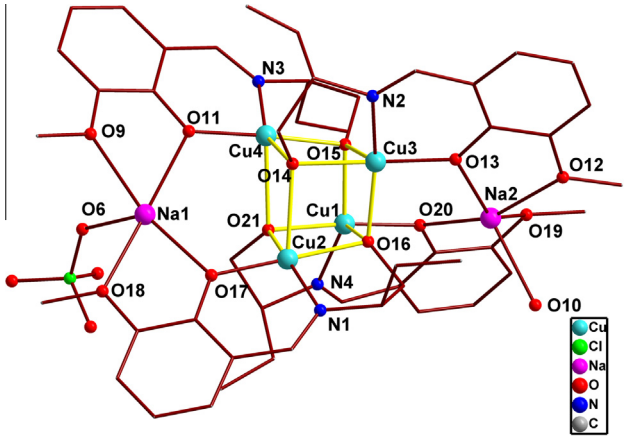

Fig. 1. Perspective views of the cationic complex unit $[Cu_4(L^1)_4Na_2(ClO_4)(H_2O)]^+$. Hydrogen atoms are omitted for clarity.

oxygens each acts as μ_3-O bridge connecting four neighboring copper(II) ions to form a $[Cu_4O_4]$ core exhibiting a cubic array of alternating copper and oxygen atoms occupying the corners of the cube. While on the two sides of the $[Cu_4O_4]$ cubane, the two deprotonated phenol oxygens each bridge to Na^+ cations with the methoxy groups providing additional chelation of the Na^+ cations, which are further ligated by a water molecule or a perchlorate anion.

Within the $[Cu_4O_4]$ cubane core, all copper(II) centers are five-coordinate with a NO_4 donor set from the Schiff base ligands. The basal plane of the square-pyramid is consisted of the phenolate oxygen atom, the imine nitrogen atom of the salicylidene fragment and two μ_3-alkoxide oxygen atoms, while the apical position is occupied by another μ_3-alkoxide oxygen atom. Cu1, Cu2, Cu3 and Cu4 are deviated from the corresponding mean planes range from 0.119 to 0.433 Å, towards the apical ligand atom. The Cu–O and Cu–N bond lengths in the equatorial plane range from 1.896 to 2.001 Å and from 1.919 to 1.932 Å (see Table 2). The apical oxygen atoms show longer Cu–O bond lengths range from 2.264 to 2.322 Å. The elongation of the Cu–O axial bonds is due to a pseudo-Jahn–Teller distortion of the d^9 copper(II) center.

Table 2
Selected bond distances (Å) and angles (°) for complex **1**.

Bond lengths (Å)			
Cu1–N4	1.919(4)	Cu3–N2	1.932(5)
Cu2–N1	1.931(4)	Cu4–N3	1.931(4)
Cu1–O3	1.991(3)	Cu3–O3	2.310(3)
Cu1–O5	1.909(3)	Cu3–O9	1.986(3)
Cu1–O6	1.995(3)	Cu3–O11	1.904(4)
Cu1–O9	2.322(3)	Cu3–O12	1.972(3)
Cu2–N1	1.931(4)	Cu4–N3	1.931(4)
Cu2–O6	1.995(3)	Cu4–O2	1.896(3)
Cu2–O8	1.907(3)	Cu4–O3	1.974(3)
Cu2–O9	1.997(3)	Cu4–O6	2.264(3)
Cu2–O12	2.288(3)	Cu4–O12	2.001(3)
Bond angles (°)			
O5–Cu1–N4	94.63(16)	O11–Cu3–N2	94.72(19)
O5–Cu1–O3	98.05(14)	N2–Cu3–O12	85.00(18)
N4–Cu1–O6	84.12(15)	O11–Cu3–O9	94.49(15)
O3–Cu1–O6	85.66(13)	O12–Cu3–O9	85.87(14)
O5–Cu1–O9	97.35(13)	O11–Cu3–O3	101.03(13)
N4–Cu1–O9	120.21(16)	N2–Cu3–O3	114.21(17)
O3–Cu1–O9	80.62(13)	O12–Cu3–O3	78.80(13)
O6–Cu1–O9	77.85(12)	O9–Cu3–O3	81.03(13)
O8–Cu2–N1	93.77(17)	O2–Cu4–N3	93.91(16)
O8–Cu2–O6	96.22(14)	N3–Cu4–O3	85.94(16)
N1–Cu2–O9	84.61(16)	O2–Cu4–O12	94.95(14)
O6–Cu2–O9	86.08(13)	O3–Cu4–O12	86.79(13)
O8–Cu2–O12	101.32(14)	O2–Cu4–O6	97.43(13)
N1–Cu2–O12	118.79(16)	N3–Cu4–O6	120.46(16)
O6–Cu2–O12	80.32(13)	O3–Cu4–O6	79.17(13)
O9–Cu2–O12	77.67(13)	O12–Cu4–O6	80.79(13)

3.2.2. Crystal structure of $[Ni_4(L^2)_4(CH_3OH)_4]$ (**2**)

The X-ray single crystal diffraction study reveals that complex **2** crystallizes in the monoclinic space group $P2_1/c$. The molecular structure of complex **2** is shown in Fig. 2, selected bond lengths

and angles are summarized in Table 3. The structure of complex **2** consists of a distorted $[Ni_4O_4]$ cubane core with alternating nickel ions and oxygen atoms occupying the corners of the cube. The μ_3-oxygen bridges among the cubane come from the deprotonated hydroxy oxygen atoms of Schiff base ligands $(L^2)^{2-}$, which were coordinated to the central metal ions in a similar tri-chelating fashion with one hydroxy oxygen atom, one phenoxy oxygen atom and one imino nitrogen atom. The peripheral ligation for Ni(II) ions in the cubane are completed by four terminal methanol ligands, which participate in intramolecular hydrogen bonding interactions (see Fig. S1. O···O distances: 2.636–2.714 Å, O···H-O angles: 165.163–169.393°) with the phenol oxygen atoms of the $(L^2)^{2-}$ ligands, along four of the six faces of the cubane. As a result, these four faces exhibit shorter Ni···Ni separations and smaller Ni–O–Ni angles.

All nickel(II) centers are six-coordinate with a NO_5 donor set from the Schiff base ligands and methanol. The basal plane of the octahedron is constructed by the phenoxy oxygen atom, the imino nitrogen atom, and two μ_3-hydroxy oxygen atoms while the apical positions are occupied by another μ_3-hydroxy oxygen atom and methanol oxygen atom. In addition, complex **2** appears to possess a slight apical elongation of the Ni(II) coordination octahedron, which occurs along the O–Ni–O vector involving the methanol and hydroxy oxygen atoms, with Ni–O (alkoxo) bonds on this vector of 2.115–2.184 Å versus 1.980–2.027 Å for the equatorial bonds. Several Ni^{II}_4 complexes with similar cubane structures have been reported previously, including examples with analogous intramolecular hydrogen-bonding interactions; although, an apical elongation is not evident in theses complexes [41,44,45].

3.2.3. Crystal structure of $[Ni_4(o\text{-vanillinate})_4(\eta^1,\mu_3\text{-}N_3)_4(CH_3OH)_4]$ (**3**)

The X-ray single crystal diffraction study shows that complex **3** crystallizes in the tetragonal space group $I4_1/a$. Each of the unit cells for complex **3** consists of a neutral discrete cubane $[Ni_4(o\text{-vanillinate})_4(\eta^1,\mu_3\text{-}N_3)_4(CH_3OH)_4]$. Some selected bond lengths and angles for complex **3** are presented in Table 4. As shown in Fig. 3, there are four nickel(II) ions bridged by four azides in end-on (EO) fashion to afford a $[Ni_4(\eta^1,\mu_3\text{-}N_3)_4]$ cubane structure. Four nickel(II) centers symmetrically related by a crystallographic four-fold axis occupy alternate cubane vertices and each of them is completed by one methanol molecule and one deprotonated o-vanillin decomposed from the Schiff base ligand H_2L^3 under the reaction condition. The nickel(II) center has a slightly distorted octahedron coordination geometry. The phenoxy oxygen O2, carbonyl oxygen O3 from o-vanillinate and two bridging azide nitrogen atoms N1 and N1A are coordinated in the basal plane of Ni1, with bond lengths varying in a range of 1.982(3)–2.067(3) Å. The axial positions are occupied by another bridging azide nitrogen N1B and methanol oxygen O4 with large bond lengths of Ni1–O4 = 2.085(3) Å and Ni1–N1B = 2.107(3) Å, which lies within the typical axial bond lengths range for octahedron nickel(II)

Table 3
Selected bond distances (Å) and angles (°) for complex **2**.

Bond lengths (Å)			
Ni1–O6	1.982(2)	Ni3–N2	1.989(3)
Ni1–N3	1.983(3)	Ni3–O12	2.157(3)
Ni1–O3	2.027(2)	Ni3–O2	2.129(2)
Ni1–O4	2.016(2)	Ni3–O3	2.208(2)
Ni1–O1	2.129(2)	Ni3–O1	2.043(2)
Ni1–O10	2.184(3)	Ni3–O8	1.992(2)
Ni2–N4	1.985(3)	Ni4–O2	2.020(3)
Ni2–O4	2.130(2)	Ni4–N1	1.994(3)
Ni2–O2	2.051(2)	Ni4–O3	2.115(2)
Ni2–O1	2.019(2)	Ni4–O4	2.042(2)
Ni2–O5	1.987(2)	Ni4–O7	1.980(2)
Ni2–O9	2.146(3)	Ni4–O11	2.176(3)
Bond angles (°)			
O6–Ni1–N3	94.50(11)	N1–Ni3–O8	93.77(11)
N3–Ni1–O4	83.52(11)	N1–Ni3–O3	83.26(11)
O6–Ni1–O3	98.24(10)	O8–Ni3–O1	99.95(9)
O4–Ni1–O3	84.51(10)	O3–Ni3–O1	84.01(9)
O6–Ni1–O1	94.38(10)	N1–Ni3–O1	103.21(11)
N3–Ni1–O1	102.49(10)	O8–Ni3–O1	94.44(10)
O4–Ni1–O1	78.98(9)	O3–Ni3–O1	78.76(10)
O3–Ni1–O1	81.87(9)	O1–Ni3–O1	82.43(9)
O6–Ni1–O10	96.55(10)	N1–Ni3–O11	89.77(11)
N3–Ni1–O10	86.79(11)	O8–Ni3–O11	95.78(11)
O4–Ni1–O10	90.64(10)	O3–Ni3–O11	91.98(11)
O3–Ni1–O10	86.51(10)	O1–Ni3–O11	82.33(10)
N4–Ni1–O5	93.48(11)	O7–Ni4–N1	93.65(11)
N4–Ni1–O1	83.48(10)	N1–Ni4–O1	83.79(11)
O5–Ni1–O1	99.20(10)	O7–Ni4–O4	98.27(10)
O1–Ni1–O1	84.98(9)	O1–Ni4–O4	85.58(9)
N4–Ni1–O4	102.66(10)	O7–Ni4–O3	91.98(10)
O5–Ni1–O4	92.19(10)	N1–Ni4–O3	104.71(11)
O1–Ni1–O4	78.88(9)	O1–Ni4–O3	79.28(9)
O1–Ni1–O4	82.57(9)	O4–Ni4–O3	81.67(9)
N4–Ni1–O9	88.85(11)	O7–Ni4–O11	99.75(11)
O5–Ni1–O9	98.98(11)	N1–Ni4–O11	86.28(11)
O1–Ni1–O9	90.89(10)	O1–Ni4–O11	89.86(10)
O1–Ni1–O9	83.65(10)	O4–Ni4–O11	85.09(10)

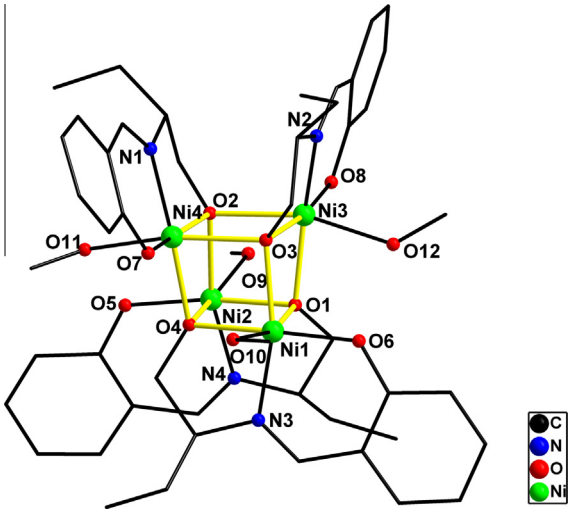

Fig. 2. Perspective views of the molecule structure of complex **2**. Hydrogen atoms are omitted for clarity.

Table 4
Selected bond distances (Å) and angles (°) for complex **3**.

Bond lengths (Å)			
Ni1–N1A	2.107(3)	Ni1–O2	1.982(3)
Ni1–N1B	2.067(3)	Ni1–O4	2.085(3)
Ni1–N1	2.067(3)	N1–Ni1A	2.107(3)
Ni1–O3	2.012(3)	N1–Ni1C	2.067(3)
Bond angles (°)			
N1–Ni1–N1A	82.51(11)	O2–Ni1–N1A	93.34(10)
N1–Ni1–N1B	81.33(11)	O2–Ni1–O3	91.57(10)
N11–Ni1–N1B	81.54(11)	O2–Ni1–O4	97.87(12)
N1–Ni1–O4	89.46(11)	O4–Ni1–N1B	168.55(11)
N11–Ni1–O4	90.58(11)	Ni13–N1–Ni1B	96.70(11)
O3–Ni1–N1B	97.45(12)	Ni1–N1–Ni1B	98.27(11)
O3–Ni1–N1	92.50(11)	Ni1–N1–Ni1C	97.97(11)
O3–Ni1–N1A	175.00(11)	N2–N1–Ni1	120.5(2)
O3–Ni1–O4	89.69(13)	N2–N1–Ni1C	119.0(2)
O2–Ni1–N1	171.63(11)	N2–N1–Ni1B	119.4(2)
O2–Ni1–N1B	90.90(10)		

Symmetry transformations used to generate equivalent atoms: A $-1/4+Y,1/4-X,9/4-Z$; B $-X,1/2-Y,+Z$; C $1/4-Y,1/4+X,9/4-Z$.

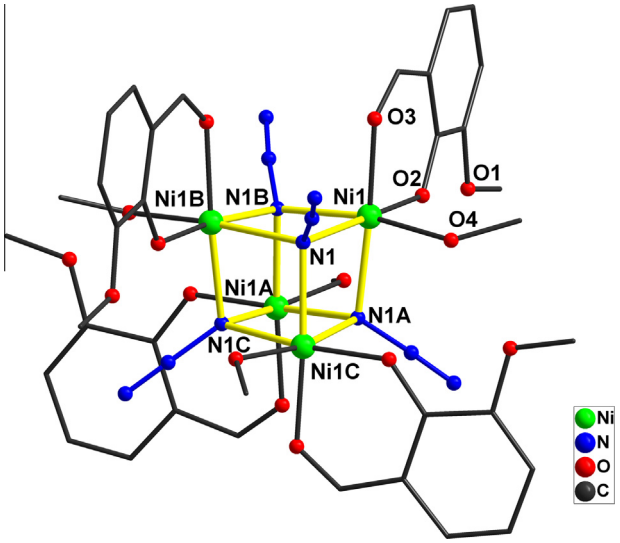

Fig. 3. Perspective views of the molecule structure of **3**. Hydrogen atoms are omitted for clarity.

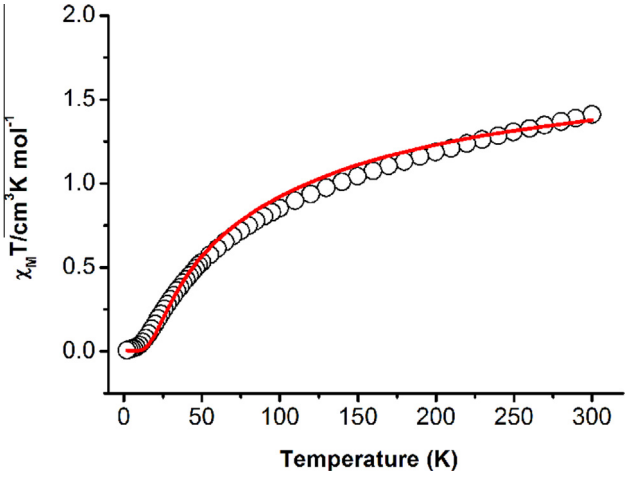

Fig. 4. $\chi_M T$ (circles) vs. T plot for complex **1**. The solid line is the best-fit line to the experimental data, see text for fitting parameters.

complexes [29,46,47]. The complex **3** reported herein can be compared to those earlier reported similar nickel(II) cubane complexes bridged by end-on doubly bridging azides [20–23] and possessing similar $[Ni_4(\eta^1,\mu_3\text{-}N_3)_4]$ cubane cores. In complex **3** cubane core, the Ni–N bond lengths are in a range from 2.067 to 2.107 Å, which are slightly shorter compare to those complexes Ni–N distances. And the N–Ni–N′ angles cover a range of 81.33(1)–82.51(1)°, the Ni–N–Ni′ angles are in a range of 96.70(1)–98.27(1)°. All the bridging angles are comparable to those previously reported for the $[Ni_4(\eta^1,\mu_3\text{-}N_3)_4]$ cubane complexes.

3.3. Magnetic properties

Magneto-structural correlations are important in understanding the magnetic coupling between the central metallic ions mediated by bridges and in designing novel molecular magnetic materials. The magnetic property of complex **1** was studied to evaluate the magnetic interactions between the four paramagnetic centers. Variable temperature magnetic susceptibility measurements from 2 to 300 K under a constant magnetic field of 5 kOe were carried out. The magnetic properties of the complex **1** as $\chi_M T$ against T plots are shown in Fig. 4. Data were corrected for gelatine capsule sample holder as well as for diamagnetic contributions. As shown in Fig. 4, the room-temperature value of $\chi_M T$ (1.38 $cm^3\,K\,mol^{-1}$) is lower than that expected for four uncorrelated spins with $S = 1/2$ ($\chi_M T = 1.5\ cm^3\,K\,mol^{-1}$ assuming $g = 2$), and $\chi_M T$ decreases slowly upon lowering of the temperature. This result indicates that there exists weak antiferromagnetic coupling interaction in the complex.

Based upon the structural features within the tetranuclear Cu_4O_4 cubane core, the magneto-structural correlation of compound **1** may be drawn successfully and it was analyzed as follows: magneto-structural correlations for the hydroxo- and l-alkoxo-bridged Cu_4O_4 cubane complexes were proposed earlier [48]. According to literature [49], there exists three major types of Cu_4O_4 cubane structures if they are classified according to the distribution of long Cu···Cu distances: (i) complexes with two short and four long Cu···Cu distances, call them (2 + 4) type; (ii) complexes with four short and two long Cu···Cu distances, and may be labeled as (4 + 2) type; and (iii) complexes where all six Cu···Cu distances are similar, and they will be termed (6 + 0) type. For complex **1**, the analysis of the structural features within the tetranuclear Cu_4O_4 cubane core (see Fig. 5) shows that the bridging system between the Cu(II) ions is quite asymmetric. As may be anticipated for five-coordinate Cu(II) ions, there are short Cu–O bond lengths corresponding to the equatorial plane and long Cu–O bonds in the axial position. This asymmetry is also obvious from the Cu···Cu separations with the Cu1···Cu2, Cu1···Cu4, Cu3···Cu2 and Cu3···Cu4 distances being significantly shorter [3.0703–3.1098 Å] than the Cu1···Cu3 and Cu2···Cu4 distances [3.2599–3.2785 Å] (see Table S1). Therefore, complex **1** clearly belongs to (4 + 2) category and the magnetic data have been analyzed considering two different magnetic coupling parameters such as J_1 for the shorter distances of Cu···Cu interactions and J_2 for the longer distances of Cu···Cu interactions (see Fig. 5). The magnetic behavior of such cubane-like cluster can be described by the Hamiltonian given in Eq. (1):

$$\hat{H} = -2J_1(\hat{S}_1\hat{S}_2 + \hat{S}_1\hat{S}_4 + \hat{S}_2\hat{S}_3 + \hat{S}_3\hat{S}_4) - 2J_2(\hat{S}_1\hat{S}_3 + \hat{S}_2\hat{S}_4) \quad (1)$$

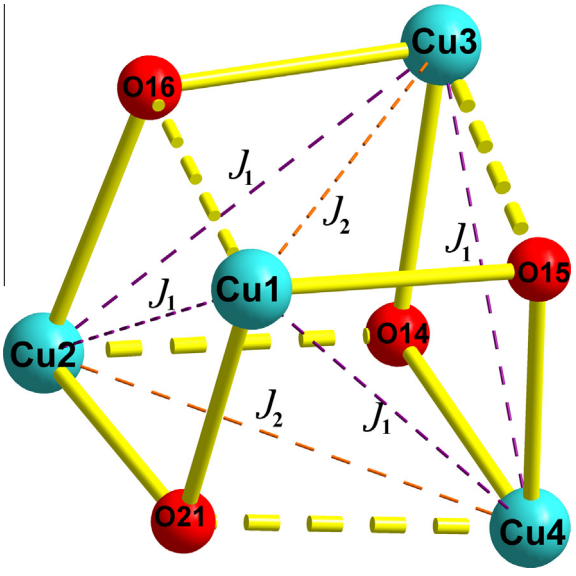

Fig. 5. Core representations of complex **1** showing the coupling scheme used in the magnetic model.

which leads to Eq. (2):

$$\chi = \frac{2Ng^2\beta^2}{kT}\frac{2\exp(J_2/kT)+\exp[(2J_2-J_1)/kT]+5\exp[(2J_2+J_1)/kT]}{1+6\exp(J_2/kT)+\exp[(2J_2-2J_1)/kT]+3\exp[(2J_2-J_1)/kT]+5\exp[(2J_2+J_1)/kT]}+N_\alpha \quad (2)$$

$N_\alpha = 240 \times 10^{-6}$ cm^3 mol^{-1}

In these expressions, J_1 and J_2 are the magnetic coupling parameters, g is the Landé factor and N, β and k have their usual meanings. Least-squares best-fit parameters are $J_1 = -23.39$ cm^{-1}, $J_2 = -16.20$ cm^{-1}, $g = 2.0$ and $R = 3.24 \times 10^{-4}$ (R is the agreement factor defined as $R = \Sigma[(\chi_M)_{obs} - (\chi_M)_{calc}]^2/\Sigma[(\chi_M)_{obs}]^2$). Noting that J_1 and J_2 are different, we want to stress here that our attempts to use a one-J model for simulation of the experimental data failed miserably.

Strong dependence of the exchange integral magnitude versus the Cu–O–Cu angle is well documented in oxo-bridged dimeric complexes. An angle of 97° marks the border between ferro- and antiferromagnetic interactions. Ferromagnetic interaction is found in complexes with smaller Cu–O–Cu angles, and antiferromagnetic interaction for larger ones [48,50]. Hence, in the case of the hydroxo-bridged Cu_4O_4 cubane complexes, an angle of 98.5° marks the border between ferro- and antiferromagnetic coupling interactions. Alkoxo-/phenoxo-bridged Cu_4O_4 cubane complexes show a similar trend: ferromagnetic interaction is found in complexes with smaller angles, and antiferromagnetic interaction for larger ones. The larger the Cu–O–Cu angle is, the stronger the antiferromagnetic coupling will be [49,51,52]. However, the interaction within our tetranuclear Cu(II) complex **1** is antiferromagnetic with the Cu–O–Cu angles in the range of 91.12–102.13°(see Table S1).

For complex **2**, variable-temperature (2–300 K) magnetic susceptibility data at a magnetic field strength of 1 KOe were collected. Plots of $\chi_M T$ versus T for **2** are shown in Fig. 6. At room temperature the product of $\chi_M T$ is 5.32 cm^3 K mol^{-1}, higher than the spin–only value of 4 cm^3 K mol^{-1} based on Ni_4 unit assuming $g = 2$. With cooling, $\chi_M T$ gradually increases reaching a maximum of 10.97 cm^3 K mol^{-1} at 7 K then quickly goes down to 9.72 cm^3 K mol^{-1} at 2 K, indicating presence of ferromagnetic coupling within Ni_4O_4 core. The sharp decrease of $\chi_M T$ value at very low temperature region may be attributed to zero-field splitting factor or weak antiferromagnetic exchange among the nickel clusters. However, the maximum of $\chi_M T$ is slightly below that expected for a ground state spin of $S_T = 4$ and a Landé factor of $g = 2.23$ obtained by Curie law ($\chi_M T = 0.125\ g^2 S_T(S_T+1) = 12.43$ cm^3 K mol^{-1}). This feature indicates the presence of antiferromagnetic coupling within Ni_4O_4 core. The temperature dependence of the reciprocal susceptibility (χ_M^{-1}) above 40 K follows the Curie–Weiss law ($\chi_M = C/(T-\theta)$) with a Weiss constant $\theta = 14.30$ K and Curie constant $C = 5.17$ cm^3 K mol^{-1}, indicating a dominated intra-cube ferromagnetic interaction. The analysis of the structural features within the tetranuclear Ni_4O_4 cubane core shows that the asymmetric topology of the cubane core for complex **2** is similar to that of complex **1** (see Fig. S2). This asymmetry is also obvious from the Ni···Ni separations with the Ni1···Ni3, Ni1···Ni4, Ni2···Ni3 and Ni2···Ni4 distances being significantly shorter [3.0348–3.0544 Å] than the Ni1···Ni2 and Ni3···Ni4 distances [3.1987–3.2020 Å] (see Table S2). Therefore the magnetic behavior for complex **2** can be described by the Hamiltonian

$$\hat{H} = -2J_1(\hat{S}_1\hat{S}_3 + \hat{S}_1\hat{S}_4 + \hat{S}_2\hat{S}_3 + \hat{S}_2\hat{S}_4) - 2J_2(\hat{S}_1\hat{S}_2 + \hat{S}_3\hat{S}_4).$$

The best fitting gave: $g = 2.23$, $J_1 = +7.23$ cm^{-1} and $J_2 = -1.84$ cm^{-1} with agreement factor of $R = \Sigma[(\chi_M)_{obs} - (\chi_M)_{calc}]^2/\Sigma[(\chi_M)_{obs}]^2 = 4.15 \times 10^{-4}$. As shown in the insert of Fig. 6, isothermal magnetization measurement does not show a saturation value. This result indicates that there exists no 3D ferromagnetic order in complex **2**.

The values of exchange-parameter are comparable to those previously reported for Ni(II) complexes with similar bridges in Ni_4O_4 cubane [23,46,53]. It would be desirable to establish a correlation between the crystal structure and the magnetic properties of these compounds, and in particular the observation of ferro- or antiferromagnetic coupling interactions. The magnetic exchange pathway is through the alkoxo-ligands which bridge each pair of metals in the cubane. It is generally accepted that the value of the M-O-M bond

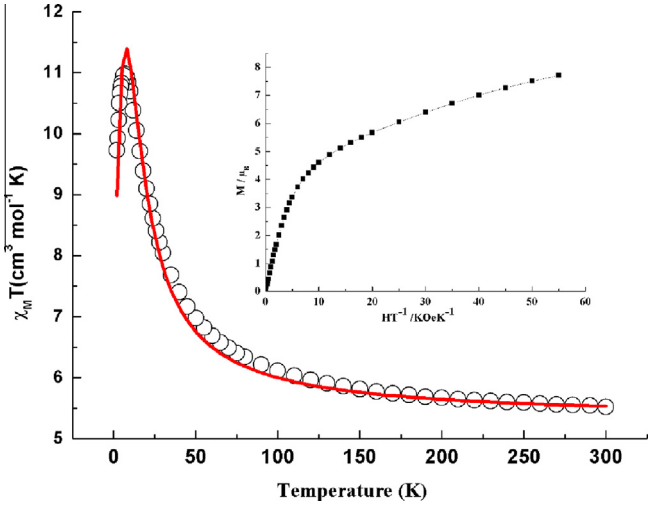

Fig. 6. $\chi_M T$ (circles) vs. T plot for complex **2**. The solid line is the best-fit line to the experimental data, see text for fitting parameters. Inset: M vs. H/T plot at 2 K for complex **2**.

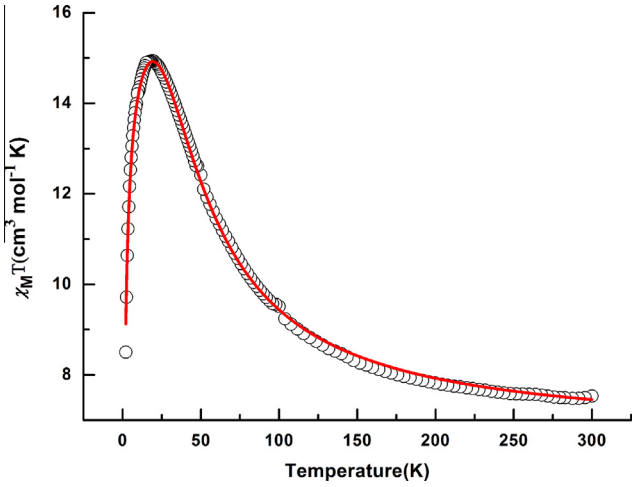

Fig. 7. $\chi_M T$ (circles) vs. T plot for complex **3**. The solid line is the best-fit line to the experimental data, see text for fitting parameters.

Table 5
Structural parameters and exchange constants for $[Ni_4(\eta^1,\mu_3\text{-}N_3)_4]$ cubane complexes.

Complex	$(Ni–N)_{av}$/Å	$(Ni–N–Ni)_{av}$/°	J (cm^{-1})	g	Ref.
$[NH(C_2H_5)_3]_8[Ni_4(dchaa)_4(N_3)_4]_2$	2.151	97.37	+55.8	2.13	[21]
$[Ni_4(N_3)_4(dbm)_4(EtOH)_4]$	2.132	97.29	+11.9	2.05	[22,23]
$[Ni_4(o\text{-vanillinate})_4(N_3)_4(CH_3OH)_4]$	2.080	97.64	+6.77	2.57	this work

H_2dchaa = 3,5-dichloro-2-hydroxy-benzylaminoacetic acid, Hdbm = dibenzoylmethane.

angle is critical in characterizing the exchange and for nickel there is a consensus that below 98–99°, the interaction will have ferromagnetic character, and above this angle it will be antiferromagnetic. For complex **2**, the average mean Ni–O–Ni angle for J_1 is 95.47° and for J_2 is 101.02° (see Table S2), thus, according to such studies the coupling is predicted to be ferro- and antiferromagnetic [54,55]. Furthermore, the ac susceptibility measurements on complex **2** were carried out in the range 2–22 K at 1000 Hz with ac field. The absence of out-of-phase ac signals above 2 K indicates that complex **2** does not behave as a SMM (see Fig. S3).

Variable-temperature magnetic study on **3** is carried out over the temperature range of 2.0–300 K and under a constant magnetic field of 1 kOe. The magnetic property of compound **3** as $\chi_M T$ against T plots is shown in Fig. 7. Data were corrected for gelatine capsule sample holder as well as for diamagnetic contributions. At room temperature, magnetic susceptibility data per $[Ni_4N_4]$ entity for **2** shows a $\chi_M T$ value of 7.46 $cm^3\ mol^{-1}$ K (see Fig. 7) which is higher than the spin only value 4 $cm^3\ mol^{-1}$ K of four non-interaction high spin Ni(II) ions (assuming $g = 2$). Plots of $\chi_M T$ versus T increase with decreasing temperature and reach a maximum at 19 K then follow by a rapidly decrease until 2 K. This behavior indicates a characteristic feature of intramolecular ferromagnetic interactions between metal centers of **3**. The sharp decrease of $\chi_M T$ value at very low temperature region may be attributed to zero-field splitting factor or weak antiferromagnetic exchange among the nickel ions centers. As is shown in the crystallographic part, the complex **3** is made up of Ni_4 entities where the azide ligand acts as a bridge to afford a cubane system (Fig. 3). The analysis of the structural features shows that the symmetric topology of the cubane core for complex **3** indicates the Ni···Ni distances in a narrow range of 3.12(6)–3.16(6) Å. Thus, we have tried to fit the magnetic property of this compound to a cubane model with the Hamiltonian

$$\hat{H} = -2J(\hat{S}_1\hat{S}_2 + \hat{S}_2\hat{S}_3 + \hat{S}_3\hat{S}_4 + \hat{S}_1\hat{S}_4 + \hat{S}_1\hat{S}_3 + \hat{S}_2\hat{S}_4)$$

where a single coupling constant, J, characterizes exchange across the six faces of the cubane [29]. A Weiss-like parameter θ has been introduced in consideration of the interactions among the tetranuclear clusters in **3**. The best fits yielded the parameters $J = 6.77\ cm^{-1}$, $g = 2.57$ and $\theta = -1.6$ K. The negative θ value reveals the presence of antiferromagnetic interactions in **3**. The high value of g reflects the spin–orbit coupling effects and orbital degeneracy of octahedral Ni(II) [56,57].

To understand the magnetic interactions of compound **3**, we were therefore interested to compare and contrast the magneto-structural properties of reported $[Ni_4(\eta^1,\mu_3\text{-}N_3)_4]$ cubane complexes. Similar magnetic behaviors have been observed for the $[Ni_4(\eta^1,\mu_3\text{-}N_3)_4]$ cubane species which display dominant ferromagnetic interactions from the nature of the binding modes through EO-azide. These behaviors are in accordance with the work of Ruiz et al. [58], for the bis- and tris-(μ-azido) Ni(II) complexes, the interaction is predicted to be ferromagnetic for all the range of θ (Ni–N–Ni) angles explored yielding a maximum at $\theta \approx 104°$ (see Table 5). Thanks to the work of Christou and co-workers [23], in the case of doubly end-on azide bridged Ni(II) species, there appears to be a trend for J to become more ferromagnetic with increasing average Ni-(μ-N) distances (see Table 5). Furthermore, the ac susceptibility measurements on complex **3** were carried out in the range 2–20 K at 1000 Hz with ac field. The absence of in-phase and out-of-phase ac signals above 2 K indicates that complex **3** does not behave as a SMM (see Fig. S4).

4. Conclusions

In summary, three cubane-type complexes have been synthesized in a facile route utilizing transition metal ions (Cu^{II} and Ni^{II}) and Schiff base ligands. Both complexes **1** and **2** have M_4O_4 cubane cores and the chelating form of the Schiff base ligands [H_2L^1 and H_2L^2]. Whereas complex **3** accompany $[Ni_4(\eta^1,\mu_3\text{-}N_3)_4]$ cubane core constructed by o-vanillin which decomposed from Schiff base ligand H_2L^3 under reaction condition. X-ray structural analysis shows the four metal ions and μ_3-bridging oxygen atoms/EO-azide bridges are located at alternating vertices of a cube. Magnetic measurements reveal that the "4 + 2" type of cubane complex **1** shows moderately strong antiferromagnetic spin exchange interactions through four μ_3-alkoxo bridge. For complex **2**, antiferromagnetic and ferromagnetic couplings coexist with a non-zero spin ground state, exhibiting dominant ferromagnetic interactions. In the case of complex **3**, the four EO-azide bridges between Ni(II) atoms transmit ferromagnetic interactions. This work shows the potential of Schiff base ligands in designing cubane geometry clusters with various transition metal ions. Furthermore, this work might be good examples for understanding the correlations between magnetic properties and bridging modes within the cubanes.

Acknowledgements

This work was financially supported by the NSFC (Nos. 21061009, 21361016) and Inner Mongolia Autonomous Region Fund for Natural Science (2013ZD09).

Appendix A. Supplementary data

CCDC 922835, 922838, 981294 contain the supplementary crystallographic data for compounds **1**, **2** and **3**. These data can be obtained free of charge via http://www.ccdc.cam.ac.uk/conts/retrieving.html, or from the Cambridge Crystallographic Data Centre, 12 Union Road, Cambridge CB2 1EZ, UK; fax: +44 1223-336-033; or e-mail: deposit@ccdc.cam.ac.uk. Supplementary data associated with this article can be found, in the online version, at http://dx.doi.org/10.1016/j.poly.2014.03.040.

References

[1] H. Ma, J.L. Petersen, V.G. Young, G.T. Yee, M.P. Jensen, J. Am. Chem. Soc. 133 (2011) 5644.
[2] X.-M. Zhang, J. Lv, F. Ji, H.-S. Wu, H. Jiao, P.v.R. Schleyer, J. Am. Chem. Soc. 133 (2011) 4788.
[3] A. Mukherjee, M. Nethaji, A.R. Chakravarty, Angew. Chem., Int. Ed. 43 (2004) 87.
[4] L. Li, Z. Liu, S.S. Turner, D. Liao, Z. Jiang, S. Yan, New J. Chem. 27 (2003) 752.
[5] M. Dey, C.P. Rao, P.K. Saarenketo, K. Rissanen, Inorg. Chem. Commun. 5 (2002) 924.
[6] C.-M. Liu, D.-Q. Zhang, D.-B. Zhu, Dalton Trans. 39 (2010) 1781.

[7] G. Chaboussant, R. Basler, H.-U. Gudel, S. Ochsenbein, A. Parkin, S. Parsons, G. Rajaraman, A. Sieber, A.A. Smith, G.A. Timco, R.E.P. Winpenny, Dalton Trans. (2004) 2758.
[8] E.J. Schelter, F. Karadas, C. Avendano, A.V. Prosvirin, W. Wernsdorfer, K.R. Dunbar, J. Am. Chem. Soc. 129 (2007) 8139.
[9] H. Miyasaka, T. Nezu, K. Sugimoto, K.-I. Sugiura, M. Yamashita, R. Clérac, Chem. Eur. J. 11 (2005) 1592.
[10] G.J.T. Cooper, G.N. Newton, D.-L. Long, P. Kögerler, M.H. Rosnes, M. Keller, L. Cronin, Inorg. Chem. 48 (2009) 1097.
[11] S. Akine, A. Akimoto, T. Shiga, H. Oshio, T. Nabeshima, Inorg. Chem. 47 (2008) 875.
[12] R. Shaw, I.S. Tidmarsh, R.H. Laye, B. Breeze, M. Helliwell, E.K. Brechin, S.L. Heath, M. Murrie, S. Ochsenbein, H.-U. Gudel, E.J.L. McInnes, Chem. Commun. (2004) 1418.
[13] J. Tang, J. Sánchez Costa, A. Pevec, B. Kozlevčar, C. Massera, O. Roubeau, I. Mutikainen, U. Turpeinen, P. Gamez, J. Reedijk, Cryst. Growth Des. 8 (2008) 1005.
[14] E.A. Buvaylo, V.N. Kokozay, O.Y. Vassilyeva, B.W. Skelton, J. Jezierska, L.C. Brunel, A. Ozarowski, Inorg. Chem. 44 (2004) 206.
[15] N. Lopez, T.E. Vos, A.M. Arif, W.W. Shum, J.C. Noveron, J.S. Miller, Inorg. Chem. 45 (2006) 4325.
[16] C.G. Efthymiou, C. Papatriantafyllopoulou, N.I. Alexopoulou, C.P. Raptopoulou, R. Boča, J. Mrozinski, E.G. Bakalbassis, S.P. Perlepes, Polyhedron 28 (2009) 3373.
[17] D. Mandal, C.S. Hong, H.C. Kim, H.-K. Fun, D. Ray, Polyhedron 27 (2008) 2372.
[18] J.-W. Ran, S.-Y. Zhang, B. Xu, Y. Xia, D. Guo, J.-Y. Zhang, Y. Li, Inorg. Chem. Commun. 11 (2008) 73.
[19] K. Isele, F. Gigon, A.F. Williams, G. Bernardinelli, P. Franz, S. Decurtins, Dalton Trans. (2007) 332.
[20] D.-Q. Ma, S. Hikichi, M. Akita, Y. Moro-oka, J. Chem. Soc., Dalton Trans. (2000) 1123.
[21] Y. Xiao, S.H. Zhang, G.Z. Li, Y.G. Wang, C. Feng, Inorg. Chim. Acta 366 (2011) 39.
[22] M.A. Halcrow, J.C. Huffman, G. Christou, Angew. Chem., Int. Ed. Engl. 34 (1995) 889.
[23] M.A. Halcrow, J.-S. Sun, J.C. Huffman, G. Christou, Inorg. Chem. 34 (1995) 4167.
[24] S. Thakurta, P. Roy, R.J. Butcher, M. Salah El Fallah, J. Tercero, E. Garribba, S. Mitra, Eur. J. Inorg. Chem. 2009 (2009) 4385.
[25] A. Sieber, C. Boskovic, R. Bircher, O. Waldmann, S.T. Ochsenbein, G. Chaboussant, H.U. Güdel, N. Kirchner, J. van Slageren, W. Wernsdorfer, A. Neels, H. Stoeckli-Evans, S. Janssen, F. Juranyi, H. Mutka, Inorg. Chem. 44 (2005) 4315.
[26] E.-C. Yang, W. Wernsdorfer, L.N. Zakharov, Y. Karaki, A. Yamaguchi, R.M. Isidro, G.-D. Lu, S.A. Wilson, A.L. Rheingold, H. Ishimoto, D.N. Hendrickson, Inorg. Chem. 45 (2005) 529.
[27] D. Maity, A.D. Jana, M. Debnath, N.G.R. Hearns, M.-H. Sie, H.M. Lee, R. Clérac, M. Ali, Eur. J. Inorg. Chem. 2010 (2010) 3484.
[28] J.K. Eberhardt, T. Glaser, R.-D. Hoffmann, R. Fröhlich, E.-U. Würthwein, Eur. J. Inorg. Chem. 2005 (2005) 1175.
[29] K.G. Alley, R. Bircher, H.U. Güdel, B. Moubaraki, K.S. Murray, B.F. Abrahams, C. Boskovic, Polyhedron 26 (2007) 369.
[30] Y. Xie, J. Ni, F. Zheng, Y. Cui, Q. Wang, S.W. Ng, W. Zhu, Cryst. Growth Des. 9 (2008) 118.
[31] M. Moragues-Cánovas, M. Helliwell, L. Ricard, É. Rivière, W. Wernsdorfer, E. Brechin, T. Mallah, Eur. J. Inorg. Chem. 2004 (2004) 2219.
[32] Y. Zhang, X.-M. Zhang, T.-F. Liu, W.-G. Xu, Transition Met. Chem. 35 (2010) 851.
[33] Y.-F. Ji, R. Wang, S. Ding, C.-F. Du, Z.-L. Liu, Inorg. Chem. Commun. 16 (2012) 47.
[34] E. Hecht, T. Rüffer, H. Lang, Z. Anorg. Allg. Chem. 630 (2004) 1326.
[35] L.-X. Xie, X. Zhang, C. Yuan, X. Li, Synth. React. Inorg., Met.-Org., Nano-Met. Chem. 39 (2009) 291.
[36] D. Saha, T. Maity, R. Bera, S. Koner, Polyhedron 56 (2013) 230.
[37] Z. Lu, T. Fan, W. Guo, J. Lu, C. Fan, Inorg. Chim. Acta 400 (2013) 191.
[38] S. Sasmal, S. Mohanta, J. Chem. Sci. 124 (2012) 1353.
[39] P. Bhowmik, N. Aliaga-Alcalde, V. Gómez, M. Corbella, S. Chattopadhyay, Polyhedron 49 (2013) 269.
[40] R. Koner, S. Hazra, M. Fleck, A. Jana, C.R. Lucas, S. Mohanta, Eur. J. Inorg. Chem. 2009 (2009) 4982.
[41] S. Hazra, R. Koner, P. Lemoine, E.C. Sañudo, S. Mohanta, Eur. J. Inorg. Chem. 2009 (2009) 3458.
[42] X. Xu, L. Zhao, G.-F. Xu, Y.-N. Guo, J. Tang, Z. Liu, Dalton Trans. 40 (2011) 6440.
[43] G.M. Sheldrick, Acta Crystallogr., Sect. A 64 (2008) 112.
[44] M. Koikawa, M. Ohba, T. Tokii, Polyhedron 24 (2005) 2257.
[45] W.-H. Zhang, N.B. Sulaiman, P.X.S. Tio, T.S.A. Hor, CrystEngComm 13 (2011) 2915.
[46] S. Shit, M. Nandy, G. Rosair, C.J. Gómez-García, J.J. Borras Almenar, S. Mitra, Polyhedron 61 (2013) 73.
[47] S.-H. Zhang, N. Li, C.-M. Ge, C. Feng, L.-F. Ma, Dalton Trans. 40 (2011) 3000.
[48] V.H. Crawford, H.W. Richardson, J.R. Wasson, D.J. Hodgson, W.E. Hatfield, Inorg. Chem. 15 (1976) 2107.
[49] J. Chakraborty, S. Thakurta, G. Pilet, D. Luneau, S. Mitra, Polyhedron 28 (2009) 819.
[50] Y.-M. Li, J.-J. Zhang, R.-B. Fu, S.-C. Xiang, T.-L. Sheng, D.-Q. Yuan, X.-H. Huang, X.-T. Wu, Polyhedron 25 (2006) 1618.
[51] E. Ruiz, P. Alemany, S. Alvarez, J. Cano, J. Am. Chem. Soc. 119 (1997) 1297.
[52] E. Ruiz, P. Alemany, S. Alvarez, J. Cano, Inorg. Chem. 36 (1997) 3683.
[53] Q. Liang, R. Huang, X. Chen, Z. Li, X. Zhang, B. Sun, Inorg. Chem. Commun. 13 (2010) 1134.
[54] J.M. Clemente-Juan, B. Chansou, B. Donnadieu, J.-P. Tuchagues, Inorg. Chem. 39 (2000) 5515.
[55] Z. Lin, Z. Li, H. Zhang, Cryst. Growth Des. 7 (2007) 589.
[56] S. Feng, M. Zhu, L. Lu, L. Du, Y. Zhang, T. Wang, Dalton Trans. (2009) 6385.
[57] S. Brooker, D.J. de Geest, R.J. Kelly, P.G. Plieger, B. Moubaraki, K.S. Murray, G.B. Jameson, J. Chem. Soc., Dalton Trans. (2002) 2080.
[58] E. Ruiz, J. Cano, S. Alvarez, P. Alemany, J. Am. Chem. Soc. 120 (1998) 11122.

Please cite this article in press as: X. Qin et al., Polyhedron (2014), http://dx.doi.org/10.1016/j.poly.2014.03.040